



# Nonmonotonic thermal histories and contrasting kinetics of multiple thermochronometers

Peter W. Reiners

*Department of Geosciences, University of Arizona, Tucson, AZ 85721, USA*

Received 7 January 2008; accepted in revised form 30 March 2009; available online 12 April 2009

---

## Abstract

Thermochronologic data are typically interpreted as point- or path-wise constraints on monotonic cooling histories. This is at least partly because allowing for the possibility of nonmonotonic thermal histories both precludes straightforward use of closure temperature ( $T_c$ ) concepts and introduces ambiguities in modeling continuous time–temperature paths from multiple thermochronometers or closure profile, multi-domain, or fission-track length data. However, the monotonic cooling assumption severely limits the ability to elucidate reheating episodes with potentially important geologic significance. Here I show that in some cases multiple thermochronometers with contrasting kinetic properties can be used to both diagnose reheating events and constrain their duration and temperature. Thermochronometric systems with varying activation energies display “kinetic crossovers,” whereby relative diffusivities are reversed at certain temperatures. For reheating events of certain durations and temperatures, this results in “inverted” ages, whereby systems with higher nominal  $T_c$ s have younger ages than systems with lower  $T_c$ s. However, even if reheating does not cause age inversion, in cases where two systems are partially reset and constraints on the timing of a reheating event are available, the relative fractional resetting extents can be inverted to estimate a square-pulse equivalent duration and temperature of the reheating event. Here I outline this approach for diagnosing nonmonotonic thermal histories and for deducing features of reheating events from thermochronometric data, and review several examples from previously published data that illustrate its use and potential in a range of applications.

© 2009 Elsevier Ltd. All rights reserved.

---

## 1. INTRODUCTION

Thermochronology relies on thermally-activated diffusion or annealing of radioisotopic daughter products. The abundance, spatial distribution, or sub-grain domain distributions of daughter products, relative to parent nuclides, (and in the case of fission tracks, their length distributions) are combined with kinetic models of diffusion or annealing to determine a range of permissible thermal histories, and in turn, timing and rates of geologic processes. Although it is generally acknowledged that this approach does not uniquely constrain thermal histories, when data from several different thermochronometers are combined, or when multi-domain, diffusion-profile, or track-length data are

available, they are often consistent with a sufficiently restricted range of thermal histories to be useful.

In many cases, however, obtaining a sufficiently restricted range of possible thermal histories requires an assumption that the sample experienced monotonic cooling. Allowing for the possibility of nonmonotonic cooling adds complexity and ambiguity to interpretations. In part this is because the concept of closure temperature ( $T_c$ ) only has significance for monotonic cooling (Dodson, 1973), but other approaches, such as those deriving continuous  $t$ – $T$  histories, are also limited if nonmonotonic histories are permitted. In many cases, especially those lacking independent  $t$ – $T$  constraints, removing the monotonic assumption significantly increases the range of potential model thermal histories. Multi-domain diffusion (MDD) modeling approaches have been developed that provide useful constraints on potential nonmonotonic cooling paths such as maximum bounds on peak temperatures associated with

---

*E-mail address:* [reiners@u.arizona.edu](mailto:reiners@u.arizona.edu)

reheating (e.g., Quidelleur et al., 1997; McDougall and Harrison, 1999; Harrison et al., 2000; Lovera et al., 2002). But fundamentally, bulk grain ages, diffusion profiles, and MDD-derived models of single thermochronometric systems are not capable of distinguishing monotonic from nonmonotonic cooling paths without additional information.

This is generally recognized in studies of sedimentary basin thermal histories, where prograde histories can be constrained to some degree by information on depositional age and timing and magnitude of burial heating, which is sometimes followed by exhumation and cooling. But often, and especially in cases of exhumation of crystalline rocks, only retrograde portions of such histories are considered, and interpretations are based on simply connecting ages and  $T_c$ s, or model  $t$ - $T$  paths, assuming monotonic cooling. This approach is clearly useful, sometimes geologically justified, and arguably most parsimonious in many circumstances. But it also neglects the possibility that some thermochronologic signatures may reflect more complex histories produced by geologically important events. The most obvious example is “partially reset” ages that reflect not only the most recent cooling path, but also prograde or earlier portions of  $t$ - $T$  histories. As an example, Fig. 1 shows just one possible nonmonotonic thermal history that is quantitatively as consistent with a hypothetical suite of thermochronometric ages as a presumably much simpler monotonic one.

Techniques for at least diagnosing, and potentially quantitatively modeling, nonmonotonic  $t$ - $T$  histories from thermochronologic data would be useful for understanding

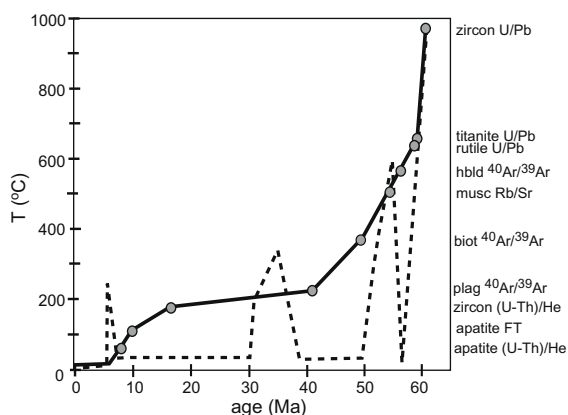


Fig. 1. Nominal closure temperature  $T_c$  (for  $dT/dt = 10$  °C/Myr) of several geo- and thermochronometers, plotted against hypothetical ages. Solid line and dashed lines represent thermal histories that predict this array of ages equally well, from forward modeling using HeFTy (Ketcham, 2005) and kinetic parameters in Table 1. The solid line represents an acceptable monotonic cooling path; the dashed line represents one of many possible histories involving several large prograde (reheating) events. Even though monotonic cooling histories may appear to be the simplest explanation for thermochronometric data, the data themselves are also consistent with a variety of nonmonotonic histories. The same principle also holds for multi-domain and spatially-resolved thermochronometric approaches such as  $^{40}\text{Ar}/^{39}\text{Ar}$  and  $^4\text{He}/^3\text{He}$ , as well as fission-track length modeling.

reheating episodes associated with a range of processes including burial, metamorphism, shear heating, or exposure to hydrothermal fluids. Several recent studies have used diffusion profiles in minerals to constrain durations of metamorphism; at least some of these require durations of peak metamorphic heating much shorter than conventionally assumed (Camacho et al., 2005; Ague and Baxter, 2007). An approach that is similar in some respects to the one presented here has also been developed for diffusion profiles in magmatic phenocrysts and the analysis of magmatic residence times (Morgan and Blake, 2006). Here I outline an approach for deducing and modeling nonmonotonic thermal histories by using contrasting kinetics of several thermochronometric systems. In certain circumstances, exploiting the differing responses of thermochronometers with different kinetic properties has the potential to both diagnose reheating events and constrain their durations and temperatures. Consideration of nonmonotonic thermal histories complicates thermochronologic interpretations in some cases, but may be particularly useful in others. It may also explain some observations previously interpreted as anomalous thermochronometric behavior, such as “inverted” thermochronometric ages – those in which systems with lower  $T_c$ s have older ages than systems with higher  $T_c$ s. For example, Fig. 2 shows predicted ages of the same array of thermochronometric systems as Fig. 1, but for a thermal history involving two separate reheating episodes. The apparently inverted ages of four different pairs of ther-

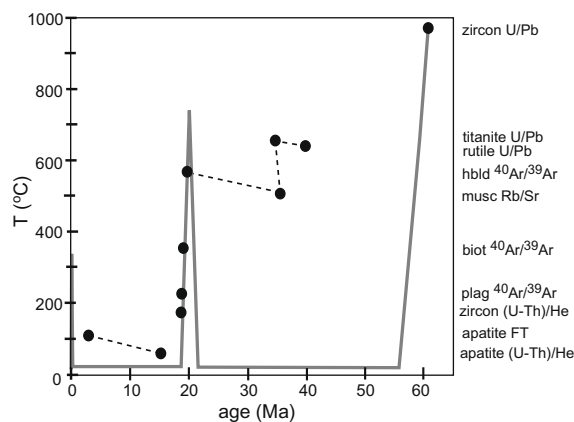


Fig. 2. Nominal  $T_c$ s of the same systems shown in Fig. 1, plotted as a function of ages that result from the thermal history shown by the solid grey line. Following rapid cooling from high temperatures ( $<900$  °C) and ending at 55 Ma, this history involves two reheating episodes from an ambient  $T$  of 25 °C: (1) to 750 °C at 20 Ma with symmetric monotonic 1-Myr pro- and retrograde paths; (2) recent (indistinguishable from zero age) heating to 350 °C for 30 min (e.g., from near surface heating by wildfire, shear, volcanism, impact-related metamorphism, etc.). This thermal history produces apparent “age inversions” among four different pairs of thermochronometers (dashed lines), whereby systems with higher  $T_c$ s have younger ages than those with lower  $T_c$ s. If interpreted in the context of monotonic cooling, such data would probably be considered unreliable for analytical or petrologic reasons. Allowing for nonmonotonic histories, these data require at least two different reheating events to produce the age inversions observed among the high- and low- $T_c$  samples.

mochronometers would be difficult to explain without considering nonmonotonic cooling, as explained below.

## 2. GENERAL APPROACH

Thermochronometric resetting of noble-gas-based systems, whether partial or complete, is typically modeled as thermally activated diffusive loss of daughter products out of a diffusion domain. Analogous equations treat the annealing of fission tracks and resetting of fission-track ages (e.g., Ketcham, 2005). In the treatment that follows and as is standard practice in most thermochronologic applications, I ignore diffusion of parent nuclides and, for noble gas systems, assume a zero concentration of daughter products at the diffusion domain boundary [for examples where the latter does not hold, see Baxter (2003) and Camacho et al. (2005)]. For simplicity, I also assume that heating events causing resetting are sufficiently brief such that daughter ingrowth during the event is negligible. This assumption is not necessarily a general requirement of this approach, however, and these methods could also be adapted for situations involving significant daughter ingrowth during reheating.

A square-pulse heating event at temperature  $T$  for duration  $t$ , yields a unique value of  $Dt/a^2$ , where  $D$  is the diffusivity of the daughter product in the diffusion domain with an effective lengthscale  $a$  (in the case of a spherical domain,  $a$  = radius). The diffusivity is assumed to follow an Arrhenius law of the form

$$\frac{D}{a^2} = \frac{D_0}{a^2} \exp[-E_a/RT], \quad (1)$$

where  $D_0$  and  $E_a$  are the experimentally determined frequency factor and activation energy, respectively, and  $R$  is the gas constant. Non-square-pulse heating events can also be treated in this context by replacing  $Dt/a^2$  with  $\tau$ , where

$$\tau(T, t) = \frac{D_0}{a^2} \int_0^t \exp\left[\frac{-E_a}{R} \frac{1}{T(t')}\right] dt'. \quad (2)$$

Equations relating  $t$  to fractional loss  $f$  have been compiled, and approximate solutions have been derived that make practical use easier (e.g., Fechtig and Kalbitzer, 1966; Crank, 1975; McDougall and Harrison, 1999, and references therein). For example, for an initially uniform concentration of daughter products within a spherical diffusion domain, the exact solution for fractional loss is

$$f = 1 - (6/\pi^2) \sum_1^{\infty} (1/n^2) \exp(-n^2\pi^2\tau), \quad (3)$$

which can be approximated by

$$f \approx 6(\tau/\pi)^{1/2} - 3\tau, \quad f \leq 0.85, \quad (4)$$

and

$$f \approx 1 - (6/\pi^2) \exp(-\pi^2\tau), \quad f \geq 0.85. \quad (5)$$

Similarly, for domains assumed to have the geometry of infinite cylinders,

$$f = 1 - 4 \sum_1^{\infty} (1/\alpha_n^2) \exp(-\alpha_n^2\tau), \quad (6)$$

where  $\alpha_n$  are roots of  $J_0(a\alpha_n) = 0$ , where  $J_0(x)$  is the Bessel function of the first kind of order zero.

This can be approximated by

$$f \approx \frac{4}{\sqrt{\pi}} \sqrt{\tau} - \tau, \quad f \leq 0.60, \quad (7)$$

and

$$f \approx 1 - \frac{9}{13} \exp(-5.78\tau), \quad f \geq 0.60. \quad (8)$$

Rearranging Eqs. (4), (5), (7), and (8) yields  $\tau$  as a function of  $f$ :

$$\text{sphere, } f \leq 0.85 : \tau = \left( \frac{1}{\sqrt{\pi}} - \frac{(9/\pi - 3f)^{1/2}}{3} \right)^2, \quad (9)$$

$$\text{sphere, } f \geq 0.85 : \tau = \frac{-1}{\pi^2} \ln \left[ (1-f) \frac{\pi^2}{6} \right], \quad (10)$$

$$\text{infinite cylinder, } f \leq 0.60 : \tau = \left( \frac{2}{\sqrt{\pi}} - \sqrt{\frac{4}{\pi} - f} \right)^2, \quad (11)$$

$$\text{infinite cylinder, } f \geq 0.60 : \tau = -0.173 \ln \left[ \frac{13}{9} (1-f) \right]. \quad (12)$$

For square-pulse heating events,  $\tau$  in Eqs. (9)–(12) can be replaced with  $Dt/a^2$  and rearranged to solve for duration  $t$  of a resetting event as a function of fractional resetting extent  $f$ , temperature  $T$ , and the kinetic parameters of the system:

$$\text{sphere, } f \leq 0.85 : \ln(t) = \ln \left\{ \left[ \frac{1}{\pi^{1/2}} - \frac{(9/\pi - 3f)^{1/2}}{3} \right]^2 \frac{a^2}{D_0} \right\} + \frac{E_a}{R} \left( \frac{1}{T} \right), \quad (13)$$

sphere,  $f \geq 0.85 : \ln(t)$

$$= \ln \left\{ -\ln \left[ \frac{\pi^2}{6} (1-f) \right] \frac{a^2}{\pi^2 D_0} \right\} + \frac{E_a}{R} \left( \frac{1}{T} \right), \quad (14)$$

$$\text{infinite cylinder, } f \leq 0.60 : \ln(t) = \ln \left\{ \left[ \frac{2}{\sqrt{\pi}} - \sqrt{\frac{4}{\pi} - f} \right]^2 \frac{a^2}{D_0} \right\} + \frac{E_a}{R} \left( \frac{1}{T} \right), \quad (15)$$

infinite cylinder,  $f \geq 0.60 : \ln(t)$

$$= \ln \left\{ \left[ -0.173 \ln \left[ \frac{13}{9} (1-f) \right] \right] \frac{a^2}{D_0} \right\} + \frac{E_a}{R} \left( \frac{1}{T} \right). \quad (16)$$

Eqs. (13)–(16) produce a family of constant- $f$  contours in plots of  $\ln(t)$  versus inverse  $T$  of hypothetical square-pulse equivalent heating/resetting events. Similar equations and resetting contours can be derived for fission-track systems.

If two different thermochronometric systems  $i$  and  $j$  are partially reset by the same heating event, one can define:

$$\frac{\tau_i}{\tau_j} \equiv \chi_{i-j}. \quad (17)$$

For an arbitrary thermal history,

$$\chi_{i-j} = \frac{D_{0i}}{D_{0j}} \frac{a_j^2}{a_i^2} \frac{\int_0^t \exp\left[\frac{-E_{ai}}{R} \frac{1}{T(t')}\right] dt'}{\int_0^t \exp\left[\frac{-E_{aj}}{R} \frac{1}{T(t')}\right] dt'}. \quad (18)$$



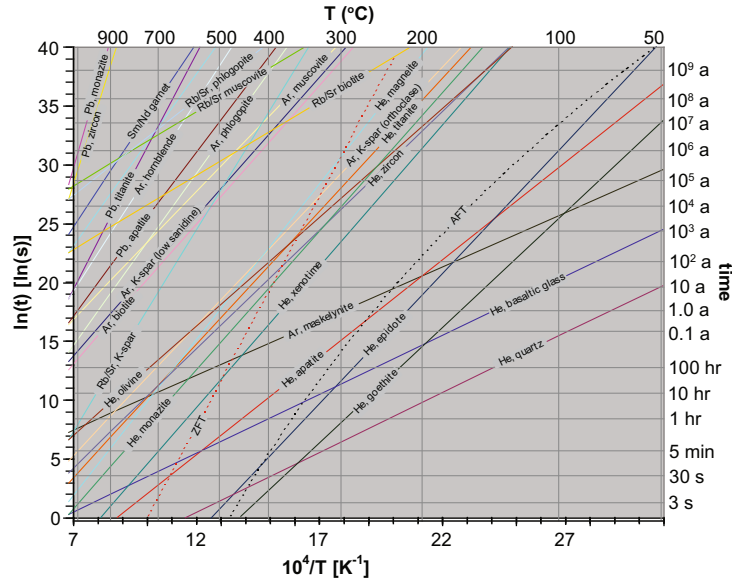


Fig. 4. Ninety-nine percent fractional loss contours of systems in Fig. 1, as a function of  $\ln(t)$  and inverse  $T$ . ZFT and AFT (zircon and apatite fission-track, respectively) contours correspond to 55% normalized track lengths (nearly complete resetting). ZFT trend uses zero-damage model kinetics of Rahn et al. (2004) as cited in Table 1. AFT trend uses fanning-curvilinear model of Ketcham et al. (1999). Contour slopes are proportional to  $E_a$  of each system. Intersecting contours correspond to kinetic crossovers. For example, a square-pulse equivalent 1-hour heating event at 400 °C would completely reset the AFT system, but only partially reset the apatite He system, even though apatite He has a lower  $T_c$  for any cooling rate.

apparently “inverted” age relationship is diagnostic of non-monotonic cooling. Further, because each system will have a family of resetting contours in this type of plot, the combined  $f_s$  for systems with different  $E_a$ s provide a unique solution for the duration and temperature of reheating (Eqs. (19)–(21), or Eq. (18) for a non-square pulse).

### 3.2. Coupling AFT and noble-gas system resetting to derive $T$ and $t$

As shown in Fig. 4, resetting contours of the apatite fission-track (AFT) system (for  $f$  greater than a few %) have steeper slopes than those of the apatite He system, reflecting a higher  $E_a$  of the AFT system. The  $T_c$  of the AFT system is also higher, so if a sample only experienced monotonic cooling, the AFT age will be older than the apatite He age. However, short duration, high-temperature reheating events (e.g., 400 °C for 1 h), may completely reset AFT ages, but only partially reset apatite He ages. Fig. 5 compares these systems in greater detail, using the He diffusion for Durango apatite (Farley, 2000) and the  $c$ -axis projected fanning curvilinear AFT annealing model (for RN apatite) of Ketcham et al. (1999). This annealing model uses a function  $g(r)$  to relate the ratio of pre- and post-heating track lengths  $r$ , to empirical parameters  $\alpha$  (−0.35878),  $\beta$  (−2.9633),  $c_0$  (−61.311),  $c_1$  (1.292),  $c_2$  (−100.53), and  $c_3$  (−8.7225) derived from experimental data:

$$g(r) = \frac{[(1 - r^\beta)/\beta]^\alpha - 1}{\alpha} = c_0 + c_1 \left[ \frac{\ln(t) - c_2}{\ln(1/T) - c_3} \right]. \quad (22)$$

Eq. (22) can be rearranged to yield  $\ln(t)$  as a function of (natural log of) inverse temperature, analogous to Eqs. (13)–(16):

$$\ln(t) = c_2 - \frac{c_3}{c_1} [g(r) - c_0] + \frac{g(r) - c_0}{c_1} \ln(1/T). \quad (23)$$

FT length reduction  $r$ , can be related to fractional track density  $\rho_s$  (i.e., one minus fractional age resetting or  $f_{AFT}$ ), by inverting the equations in Ketcham (2005):

$$\text{if } \rho_s \geq 0.612, r = (\rho_s + 0.6)/1.6; \quad (24)$$

$$\text{if } \rho_s < 0.612, r = 0.4974 + \frac{\sqrt{0.30642 + 36.82\rho_s}}{18.41} \quad (25)$$

A minor detail is that, as suggested by Ketcham (personal communication), a cutoff  $\rho_s$  of 0.612 is used here, instead of 0.624 as in Ketcham (2005). The resetting contours for constant  $f_{AFT}$  that result from Eqs. (22)–(25) are curved in a plot of  $\ln(t)$  versus  $(1/T)$  (Fig. 5) because the apparent  $E_a$  of AFT annealing is not independent of track length reduction  $r$ , and Eqs. (22) and (23) go with  $\ln(1/T)$  instead of  $(1/T)$  as in the noble gas systems.

Fig. 5 shows the potential for multiple thermochronometric systems to constrain duration and temperature of heating events resulting in resetting. Although this figure focuses on the apatite He and FT systems, the same principles apply to any two systems with contrasting  $E_a$ . Heating events resulting in full resetting of the higher  $E_a$  system (AFT) but only partial resetting of the lower  $E_a$  system (apatite He) must lie on a  $t$ – $T$  contour corresponding to the  $f$  of the lower  $E_a$  system. If, however, both systems are partially reset, the intersection of the two fractional loss contours provides an estimate of the duration and temperature of a square-pulse equivalent heating event, as described in Eqs. (19)–(21). Although this last statement is true regardless of which system is more strongly reset, if the higher  $E_a$  system is more strongly reset than the lower

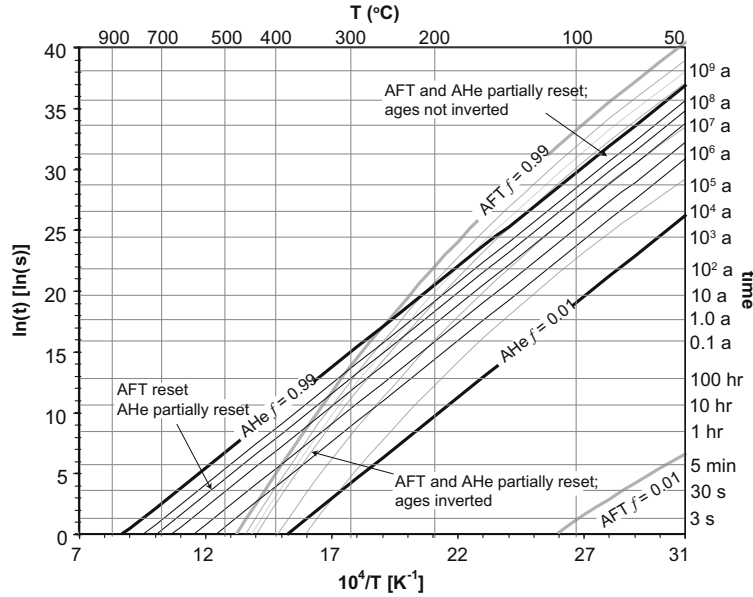


Fig. 5. Fractional resetting plot for He diffusion (solid lines) and fission-track annealing (grey lines) in apatite, using Durango apatite kinetics (Farley, 2000) with  $a = 60 \mu\text{m}$  for apatite He, and the curvilinear fanning model (RN composition) of Ketcham et al. (1999), with AFT  $f = 1 - \rho_s$  (see text) for FT. Bold lines are 1% and 99% fractional loss or annealing contours; others are 10%, 20%, 40%, 60%, and 80%. Although the AFT system has a higher nominal  $T_c$  (Table 1), relatively high- $T$ , short- $t$  heating events can produce complete resetting of the AFT system with only partial resetting of the AHe system, or greater extents of partial resetting of the AFT system than AHe system.

$E_a$  system, the inverted ages of these systems (relative to expectations based on monotonic cooling) also diagnose the existence of the reheating event, whose  $t$ - $T$  characteristics can be determined from the fractional losses. In contrast, in the absence of additional information, stronger partial resetting of the lower  $E_a$  system is equally consistent with monotonic cooling.

Combining Eqs. (23)–(25) with Eqs. (13) and (14) (or (15) and (16) for cylindrical diffusion domains) provides equations analogous to Eqs. (19)–(21). In other words,  $\rho_s$  and  $f$  of partially reset FT and noble-gas systems can be combined to yield  $t$  and  $T$  of an square-pulse equivalent heating event responsible for the resetting (Fig. 6). This is simplified with a series of substitutions grouping terms in the above equations:

$$m = c_2 - \frac{c_3}{c_1} [g(r) - c_0], \quad (26)$$

$$n = \frac{g(r) - c_0}{c_1}, \quad (27)$$

$$s = \left[ \frac{1}{\pi^{1/2}} - \frac{(9/\pi - 3f)^{1/2}}{3} \right]^2, \quad (28)$$

and

$$v = -\ln \left[ \frac{\pi^2}{6} (1 - f) \right] \frac{1}{\pi^2}. \quad (29)$$

Eqs. (26) and (27) combine terms from Eq. (23), and Eqs. (28) and (29) combine terms from Eqs. (13) and (14), respectively. Using these substitutions and combining Eqs. (23) with (28) and (29) and rearranging yields two equations for inverse  $T$ .

$$f \leq 0.85 : \frac{1}{T} = \exp \left[ \frac{1}{n} \left[ \ln \left( s \frac{a^2}{D_0} \right) + \frac{E_a}{R} \left( \frac{1}{T} \right) - m \right] \right], \quad (30)$$

and

$$f \leq 0.85 : \frac{1}{T} = \exp \left[ \frac{1}{n} \left[ \ln \left( v \frac{a^2}{D_0} \right) + \frac{E_a}{R} \left( \frac{1}{T} \right) - m \right] \right]. \quad (31)$$

The corresponding duration of a square-pulse equivalent heating event can then be calculated from Eqs. (20) or (23). Eqs. (30) and (31) can be solved iteratively. Using a linear FT annealing model (e.g., Laslett et al., 1987) allows for explicit solution of  $T$ , but this models lead to significantly different results at high- $T$  and low- $t$ , and the Ketcham et al. (1999) model is considered more accurate. Convergence of Eqs. (30) and (31) is not strongly dependent on the initial  $T$  in the first iteration, but it is slow or does not occur for low extents of fractional resetting  $f_{AFT}$  or  $(1 - \rho_s)$  of the AFT system (e.g.,  $f_{AFT}$  less than approximately 0.1–0.15), especially when fractional resetting of the noble-gas system is also high. The specific combinations of fractional resetting values where this becomes a problem depends on the specific kinetics of the two systems, but for the Renfrew and Durango apatite kinetics for AFT and the apatite He (AHe) systems, respectively, it occurs when  $f_{AFT}$  is less than approximately 0.05, but also when  $f_{AFT}$  is as high as 0.1–0.2 if  $f_{AHe}$  is greater than about 0.75. Fortunately, these combinations of fractional resetting are only caused by events with relatively long durations and low temperatures (dark blue colors in Fig. 6), which is outside the domain where these simple models neglecting syn-reheating daughter in-growth apply.

The approach outlined here for calculating durations and temperatures of a reheating event requires inferring

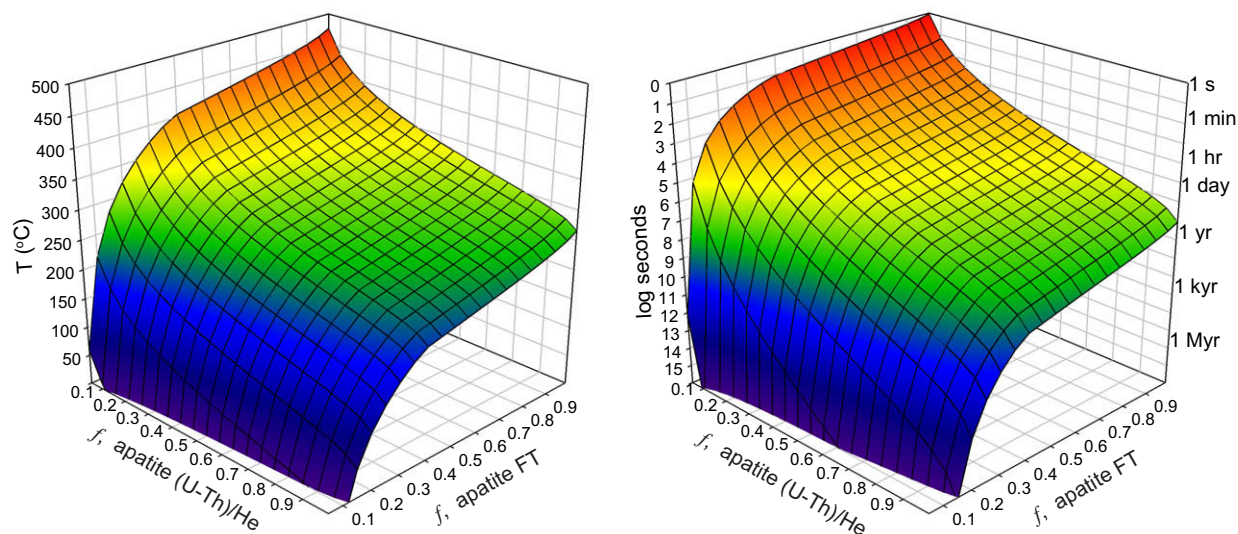


Fig. 6. Temperature and time of square-pulse heating events responsible for coupled fractional resetting extents of the apatite He (Table 1) and AFT (Ketcham et al., 1999) systems.

fractional resetting extents  $f$ , of the chronometers from their observed ages  $t$ , their pre-reheating-event ages  $t_i$ , and timing of the reheating event  $t_r$ ,

$$f = 1 - \frac{t - t_r}{t_i - t_r}. \quad (32)$$

This is simplest when heating was either recent ( $t_r = 0$ ), or when the post-heating temperature was sufficiently low so that the ages of both systems increased by the same amount. In cases where post-reheating temperatures are high enough to cause differential age accumulation in the systems, additional constraints are required to convert ages to inferred fractional losses. This approach also assumes that the duration of the reheating event was short relative to the pre-reheating-event age of the thermochronometers  $t_i$ , so that daughter ingrowth during the event is negligible. However, although it would add additional complexities and require additional assumptions, this approach could be extended to allow for daughter ingrowth and loss during the reheating event. Estimating the pre-reheating-event age  $t_i$ , may also be difficult in some tectonic settings, such as those where the regional extent of the event prevents dating a sample unaffected by the event.

Finally, the fractional loss equations for noble gas systems used here assume an initially uniform concentration daughter products across the diffusion domain, which for simplicity is assumed here to be the crystal or grain. This condition is not met for He-based systems, simply because of alpha-ejection from the crystal rim (Farley et al., 1996), but its effect on fractional degassing extents is likely to be minor, especially for samples with fractional resetting extents greater than a few percent. More importantly, this condition will also not be met for samples that have experienced slow-cooling or were previously partially reset. However, the longer a sample has resided at low temperatures

where daughter retention is nearly complete, following this earlier history, the less important this assumption becomes, because daughter product concentrations increase everywhere in the crystal including the rim (except for alpha-ejection effects) at nearly the same rate.

Uncertainties in the temperatures and durations of reheating events derived from this approach will depend primarily on uncertainties in  $f$  (and in turn on  $t$ ,  $t_i$ , and  $t_r$ ), and uncertainties in the kinetic models and parameters for diffusion and/or annealing models. The iterative calculation required for coupled solution of the fanning-curvilinear model for fission-track annealing with the noble-gas diffusion unfortunately makes error propagation non-trivial for the examples shown here. No quantitative analysis of the effects of these uncertainties is presented here, but the effects of these uncertainties on calculated square-pulse equivalent temperatures and durations are likely to be large. Beyond this, it should also be mentioned that other possible explanations for age inversions besides short-duration reheating events should be considered, including those involving violation of common thermochronologic assumptions (e.g., “excess” radiogenic daughter product, recrystallization, analytical problems, etc.).

### 3.3. Non-square-pulse heating events

Most natural reheating events are not isothermal square pulses. A simple forward modeling approach outlined here can be used to find non-square-pulse heating events consistent with coupled fractional resetting indices. Consider two systems, apatite (U–Th)/He and maskelynite  $^{40}\text{Ar}/^{39}\text{Ar}$  (Table 1, but with  $a$  for apatite He = 38  $\mu\text{m}$ , after Min and Reiners (2007)), that experience a 1-hour, 400  $^\circ\text{C}$  square-pulse reheating event. Although the maskelynite Ar system has a lower  $T_c$  than apatite He, because of its

Table 1  
Kinetic parameters of thermochronometers, estimated from experimental data.

System	$E_a$ [kJ/mol]	$\ln(D_0/a^2)$ [ln(s <sup>-1</sup> )]	$a$ for $D_0$ (μm)	$D_0$ (cm <sup>2</sup> /s)	$a$ for $f$ (μm)	$T_c$ (°C)
Monazite (U–Th)/Pb (Cherniak et al., 2004)	590	n/a	n/a	9.40E + 03	75	1018
Zircon (U–Th)/Pb (Cherniak and Watson, 2001)	544	n/a	n/a	7.80E + 02	75	974
Rutile (U–Th)/Pb (Cherniak, 2000)	243	n/a	n/a	1.60E – 06	75	624
titanite (U–Th)/Pb (Cherniak, 1993)	331	n/a	n/a	1.10E + 00	250	645
Apatite (U–Th)/Pb (Cherniak et al., 1991)	230	n/a	n/a	2.00E – 04	75	473
Garnet Sm–Nd (Ganguly et al., 1998)	258	n/a	n/a	4.70E – 05	500	690
Hornblende <sup>40</sup> Ar/ <sup>39</sup> Ar (magnesiobhd) (Harrison, 1981)	268	n/a	n/a	6.00E – 02	750	569
Phlogopite <sup>40</sup> Ar/ <sup>39</sup> Ar (Giletti, 1974)	243	n/a	n/a	7.50E – 01	750	459
Muscovite <sup>40</sup> Ar/ <sup>39</sup> Ar (Robbins, 1972)	180	n/a	n/a	4.00E – 04	750	393
Biotite <sup>40</sup> Ar/ <sup>39</sup> Ar (Grove and Harrison, 1996)	197	n/a	n/a	7.50E – 02	750	358
Kspar <sup>40</sup> Ar/ <sup>39</sup> Ar (low sanidine) (Wartho et al., 1999)	197	n/a	n/a	3.70E – 02	750	357
Kspar <sup>40</sup> Ar/ <sup>39</sup> Ar (orthoclase) (Foland, 1994)	183	n/a	n/a	9.80E – 03	10	222
Maskelynite <sup>40</sup> Ar/ <sup>39</sup> Ar (Weiss et al., 2002)	76.8	–1.9	50	3.74E – 06	50	6
Kspar Rb/Sr (Cherniak and Watson, 1992)	284	n/a	n/a	5.97E + 00	10	396
Musc Rb/Sr (Jenkin, 1997)	105	n/a	200	9.00E – 12	750	521
Plag Rb/Sr (Jenkin et al., 1995)	247.1	n/a	200	2.50E – 02	750	521
Biot Rb/Sr (Jenkin et al., 1995)	105	n/a	200	2.00E – 09	750	337
Fluorophlogopite (Hammouda and Cherniak, 2000)	136	n/a	n/a	2.70E – 10	750	581
Xenotime (U–Th)/He (Farley, 2007)	200	n/a	n/a	2.98E + 03	50	176
Titanite (U–Th)/He (Reiners and Farley, 1999)	188	n/a	n/a	5.90E + 01	250	212
Zircon (U–Th)/He (Reiners et al., 2004)	168	n/a	n/a	4.60E – 01	75	184
Apatite (U–Th)/He (Farley, 2000)	138	n/a	n/a	3.16E + 01	60	69
Apatite big	138	n/a	n/a	3.16E + 01	100	76
Apatite small	138	n/a	n/a	3.16E + 01	30	60
Epidote (U–Th)/He (Nicolescu and Reiners, 2005)	184	27.0	1500	1.15E + 10	1500	86
Monazite (U–Th)/He (Farley, 2007)	196	n/a	n/a	1.48E + 02	75	200
Goethite (U–Th)/He (Shuster et al 2005)	163	26	0.5	4.89E + 02	0.5	51
olivine (U–Th)/He (Shuster et al., 2003)	154	3	690	9.56E – 02	250	187
quartz (U–Th)/He (Shuster and Farley 2005)	84.5	11.1	430	1.22E + 02	500	–48
Magnetite (U–Th)/He (Blackburn et al., 2007)	220	15.7	250	4.11E + 03	250	247
Basaltic glass (U–Th)/He (Kurz and Jenkins 1981)	83.3	n/a	n/a	6.72E – 01	500	–24
Basaltic glass big (U–Th)/He	83.3	n/a	n/a	6.72E – 01	1000	–16
Basaltic glass small (U–Th)/He	83.3	n/a	n/a	6.72E – 01	100	–42
AFT (Ketcham et al., 1999, as cited in R&B, 2006)	147	10.5*				115
ZFT (zero-damage model, Rahn et al., 2004 as cited in R&B, 2006)	321	27.7*				342
Apatite, <sup>4</sup> He = 10 <sup>-1</sup> nmol/g (Shuster et al., 2006)	121	9.87	60	6.96E – 01	60	53
Apatite, <sup>4</sup> He = 1 nmol/g (Shuster et al., 2006)	125	10.6	60	1.43E + 00	60	58
Apatite, <sup>4</sup> He = 10 nmol/g (Shuster et al., 2006)	133	11.8	60	4.97E + 00	60	69
Apatite, <sup>4</sup> He = 10 <sup>2</sup> nmol/g (Shuster et al., 2006)	142	12.5	60	1.01E + 01	60	87
Apatite, <sup>4</sup> He = 10 <sup>3</sup> nmol/g (Shuster et al., 2006)	148	11.5	60	3.56E + 00	60	109

Notes: “ $\ln(D_0/a^2)$ ” is listed for systems for which  $D_0$  and  $a$  were not reported separately in the literature. “ $a$  for  $D_0$ ” is the effective radial dimension used to calculate  $D_0$ , if  $D_0$  and  $a$  were not reported separately. “ $a$  for  $f$ ” is the effective radial dimension used in this study for calculating  $T_c$  and fractional resetting extents  $f$ . “ $T_c$ ” is Dodson’s (1973) closure temperature. “R&B, 2006” is Reiners and Brandon (2006). AFT and ZFT are apatite and zircon fission-track. \* $\ln(D_0/a^2)$ ” for AFT and ZFT are  $\ln(\Omega/55)$ , as discussed in R&B (2006). Micas assume cylindrical diffusion domain; all other systems assume spherical.

relatively low  $E_a$ , short duration reheating produces less resetting than in the apatite He system (8%, compared with 86% for apatite He), resulting in “inverted” ages of these two systems.

We seek non-square-pulse  $t$ – $T$  histories that yield similar  $f$ s as the square-pulse event, and comparisons between them and the square-pulse equivalent history. An infinite variety of forms are conceivable, but two easily parameterized ones

are “triangular” and “impulse”. The triangular history is defined by a maximum  $T_m$  and a total duration  $t_d$  over which temperature increases and then decreases linearly and symmetrically with respect to time. In the impulse history,  $T_m$  is reached instantaneously at the beginning of the history, and  $T$  decreases exponentially as  $T = T_m e^{-\lambda t}$ , where  $\lambda = -\ln(0.01)/t_{ch}$ , and  $t_{ch}$  is the duration over which  $T$  decreases to 1% of  $T_m$ .

Fractional resetting resulting from triangular and impulse thermal histories of varying  $T_m$  and timescales were calculated by discretizing  $t$ - $T$  histories and numerically integrating Eq. (2), then calculating  $f_s$  using Eqs. (9) and (10). Residual mismatches  $R$ , to  $f_s$  of both systems, compared with those predicted by the square-pulse history, were calculated as square of sum of the squares of the differences of the  $f_s$ :

$$R = \sqrt{(f_s^1 - f_{ns}^1)^2 + (f_s^2 - f_{ns}^2)^2}, \quad (33)$$

where the superscripts refer to thermochronometric systems 1 and 2,  $f_s$  is extent of resetting predicted by the square-pulse heating event, and  $f_{ns}$  is that predicted by either the triangular or impulse heating events.

Fig. 7 shows residuals on  $f_s$  as a function of the timescales and temperatures of modeled non-square-pulse thermal histories, and best-fit histories. The maximum temperatures of these best-fit triangular or impulse heating events are higher than those of square-pulse heating events by about 30–60 °C, and the total durations (or characteristic timescales) are longer by about a factor of 5–20. This is because the non-square-pulse histories spend a relatively short duration at  $T_m$ , where diffusion is most rapid. This is compensated in the  $Dt/a^2$  term by both higher  $T_m$  and longer durations at elevated temperature. This exercise shows that, if there is reason to prefer a non-square-pulse history as more realistic than square-pulse, simplified non-square-pulse thermal histories can be deduced from combined fractional-resetting relations, and at least in some cases these provide  $T_m$  and characteristic timescales that are not extremely different from square-pulse histories. In general, however, square-pulse equivalent histories will underestimate maximum temperatures and durations.

## 4. EXAMPLES

### 4.1. Introduction

Fig. 4 shows several kinetic crossovers of thermochronometric systems with potential utility to constrain  $t$ - $T$  characteristics of reheating events across a range of characteristic durations and temperatures. Helium in basaltic glass and Ar in maskelynite both have relatively low  $E_a$ , for example, leading to resetting contours that intersect those of other systems over a wide range of temperatures and timescales. Similar to apatite, the zircon FT system has a relatively high  $E_a$  that intersects many other systems at temperatures of ~300–400 °C and timescales of  $10^1$ – $10^6$  yr. It should also be noted that, except for FT systems, fractional resetting contours depend on diffusion domain size, which in most cases is the physical grain size. In at least some cases, the utility of the approaches outlined here may be enhanced by analyzing grains of varying size.

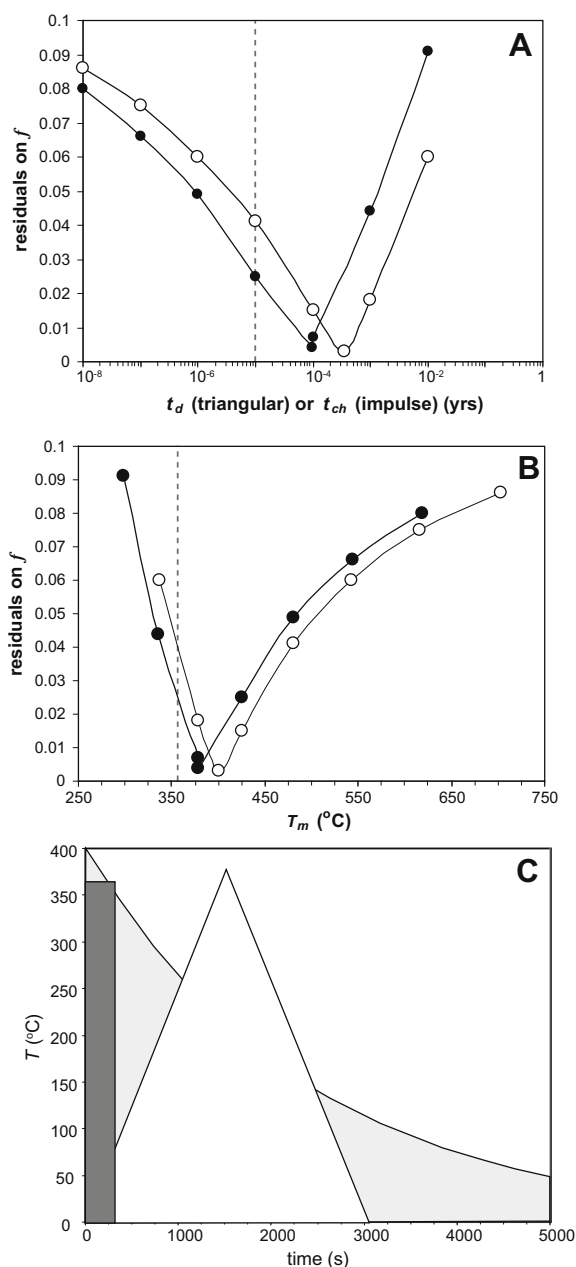


Fig. 7. Comparisons between triangular (filled circles) or impulse (open circles) heating events to square-pulse equivalent heating events, based on fractional resetting combinations of the apatite He and maskelynite Ar systems (Table 1, but with  $a = 38 \mu\text{m}$  for apatite He), and an assumed square-pulse event of 400 °C for 1 hour. (A) Residuals (Eq. (33)) on fit of heating event for varying duration  $t_d$ , of a triangular heating event, or characteristic time  $t_{ch}$  (exponential decay to 1% of maximum temperature  $T_m$ ), of impulse event. Dashed line is duration of square-pulse event. (B) Residuals for varying  $T_m$  of the triangular and impulse events. Dashed line is  $T$  of square-pulse event. (C)  $T$ - $t$  histories of the two best-fit non-square-pulse events compared with the square-pulse event. Using the approach outlined here, solving for  $t$  and  $T$  of square-pulse heating events will in general yield underestimated maximum  $T_s$  and durations of possibly more realistic non-square-pulse events.

Here I outline several examples of the importance of thermochronologic kinetic crossovers in nonmonotonic

$t$ - $T$  histories. The first interprets data from recent studies of wildfire effects, inverting single crystal He-FT double dates for square-pulse equivalent heating histories, and showing an example of how this could be extended to understanding  $t$ - $T$  histories adjacent to other types of transient heat sources such as hydrothermal veins or magmatic dikes. The second reviews an application to meteorite thermal histories, illustrating the potential utility of this approach in extraterrestrial materials. The third evaluates implications of a recently proposed radiation-damage He diffusion model for interpretation of apatite thermochronology in the case of nonmonotonic thermal histories. The fourth briefly explores the potential utility of this general approach in deducing metamorphic histories, using the apparently low  $E_a$  of Sr diffusion in micas.

#### 4.2. Wildfire

Mitchell and Reiners (2003) and Reiners et al. (2007) measured He and FT ages of apatite crystals from samples of granitoid rock taken at varying depths from a surface exposed to wildfire(s), and from thin (1–3 cm thick) detrital chips of granitic rock on the forest floor. They documented partial to complete resetting of both systems consistent with geologically recent wildfire heating. In the transect samples, the magnitude of resetting decreases towards the interior of the rock, with “fresh” unreset apatite He and FT ages of  $\sim 20$  and  $\sim 50$  Ma, at distances more than 3 cm from the exposed surface. They also observed extensive partial to com-

plete resetting of apatite He and FT ages in the detrital rock chips.

Fig. 8 shows data from the Reiners et al. (2007) study (one additional point inadvertently omitted in the original reference is included here), showing that many of the apatite crystals have FT ages younger than He ages, as predicted for short-duration, high-temperature heating (Fig. 4; Reiners et al., 2007). Using the methods outlined above, the combined ages of most of these crystals can be inverted for temperatures and durations of square-pulse equivalent heating events using equations 20, 30, and 31. Initial FT and He ages ( $t_i$ ) of 50.3 and 20.1 Ma, respectively, were assumed;  $t_r$  was assumed to be zero. He diffusion parameters were calculated from the Shuster et al. (2006) model assuming 20 Myr of ingrowth of  $^4\text{He}$ , average U and Th concentrations of the grains, and  $a = 60 \mu\text{m}$ , but using conventional Durango kinetics produces very similar results.

Inverted square-pulse  $t$ - $T$  histories for crystals that are partially reset for both systems are shown as circles in Fig. 9. Most of the grains in this example are very strongly reset for the AFT system, which is primarily an artifact of the grain selection process used in the Reiners et al. (2007) study, which mostly targeted strongly AFT-reset grains to demonstrate kinetic age inversions. A more useful sampling protocol for this study would select grains exhibiting a wide range of resetting extents for both systems. Most of the crystals require square-pulse equivalent events with temperatures of  $\sim 300$ – $425^\circ\text{C}$  and durations of several seconds to a few hundred hours. As reviewed by Mitchell

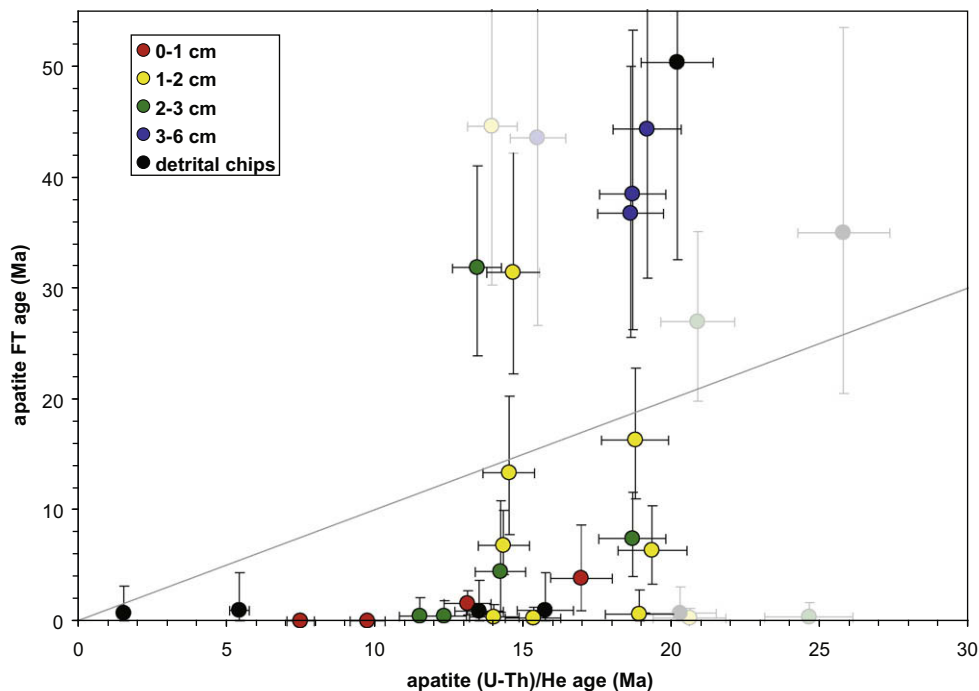


Fig. 8. Apatite FT and He ages of single crystals from a 6-cm transect in exposed bedrock, and detrital chips on the soil surface subjected to wildfire heating. Most of these are the same data in Reiners et al. (2007), but an additional point erroneously omitted from the earlier work has been added here (0–1 cm grain with  $\sim 17$ -Ma apatite He age). Six partially masked points are not used in inversion calculations, either because one or more ages is older than the assumed initial He or FT age of the samples, or yield  $t$  and  $T$  that are unrealistically low and high, respectively (two points to upper left).

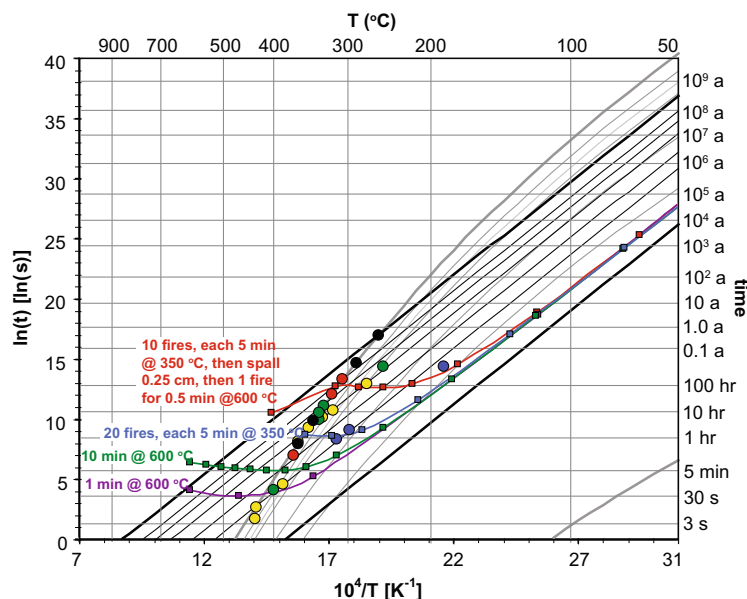


Fig. 9. Log duration and inverse temperature of square-pulse heating events calculated from inverting fractional resetting extents of wildfire-affected apatite crystals shown in Fig. 8 (colored circles), fractional resetting contours for the apatite He and AFT systems (grey and black lines), and four example model trends of square-pulse equivalent temperatures and durations predicted for samples at various depths (2.5-mm intervals; farthest left is surface), for different surface-heating scenarios (colored squares and trends). Apparent square pulse heating durations and temperatures for samples farther from the exposed surface imply much longer durations and lower temperatures than surficial heating events, because they also reflect long durations at ambient conditions, here estimated as 35 Myr at 10 °C. No single fire history, including those involving multiple events and spallation episodes, produces a trend of square-pulse equivalent heating event effects that explains the full range of single-grain data observed in this transect. This may be due to variable heating histories on the relatively large (~200 cm<sup>2</sup>) area of each analyzed slab.

and Reiners (2003), single wildfire events produce temperatures as high as ~700 °C for up to a few minutes near exposed rock margins, and less than 100–200 °C for tens of minutes to hours a few centimeters from the margins.

Given the decadal fire recurrence interval in this region (Mitchell and Reiners, 2003) and the possibility of episodic spallation, there is no reason to think that any of these samples record a single wildfire heating event. Furthermore, the approximate area of the exposed surface of the sample was roughly 200 cm<sup>2</sup>, so it is possible that the thermal dose experienced by any grain varies across the exposed surface as well as with depth from it. These factors may explain both the wide range of apparent temperatures and durations and the fact that some grains yield apparent events well outside the range of characteristic temperatures and durations of single wildfire events (Fig. 9).

The predicted effects of wildfire events of varying duration and temperatures on crystals at various depths beneath the surface were modeled using a finite difference scheme and a thermal diffusivity of 0.01 cm<sup>2</sup>/s. Thermal histories of samples at varying depths were then converted to fractional resetting extents, and the corresponding  $\tau$ 's were combined to derive apparent square-pulse equivalent heating events, using the procedure outlined above. Especially for samples more than a few millimeters from the surface, the predicted  $\tau$ 's must incorporate the effects of not only the wildfire heating, but also the preceding long-term residence at ambient near-surface, low temperature conditions, estimated here as 35 Myr of isothermal holding at 10 °C (the precise choice

of ambient conditions is not critical to these results). Fig. 9 shows the model apparent durations and temperatures of square-pulse heating equivalents that would be recorded by samples at 2.5 mm intervals beneath the exposed surface, for four different wildfire scenarios (squares). For the three scenarios without spallation, the shallowest sample (farthest left in each trend) simply records the temperature and duration of the model surficial square-pulse heating event. Samples at progressively greater depths yield lower apparent temperatures, and durations that first decrease and then increase, following a trend towards the assumed ambient temperature and holding duration. The scenario involving multiple fires and a single spallation event show that the form of these predicted trends can be complex, because the shallowest sample will reflect a combination of the temperatures and durations of events affecting it.

Fig. 9 illustrates several points about interpretation of apparent square-pulse heating events from related samples. First, the predicted temperature-duration trends for spatially related samples subject to reheating event(s) extends from the conditions at the locus of reheating (or near it, in the spallation case) to ambient conditions, with intermediate distance samples yielding apparent temperatures and durations much lower and longer, respectively, than the surficial reheating event itself. For example, all scenarios predict that weakly reset samples from certain depths (between 1–3 cm depending on the scenario) will yield apparent square-pulse equivalent temperatures of ~100–200 °C and durations of hundreds of hours to years. Second, although some of the dispersion in

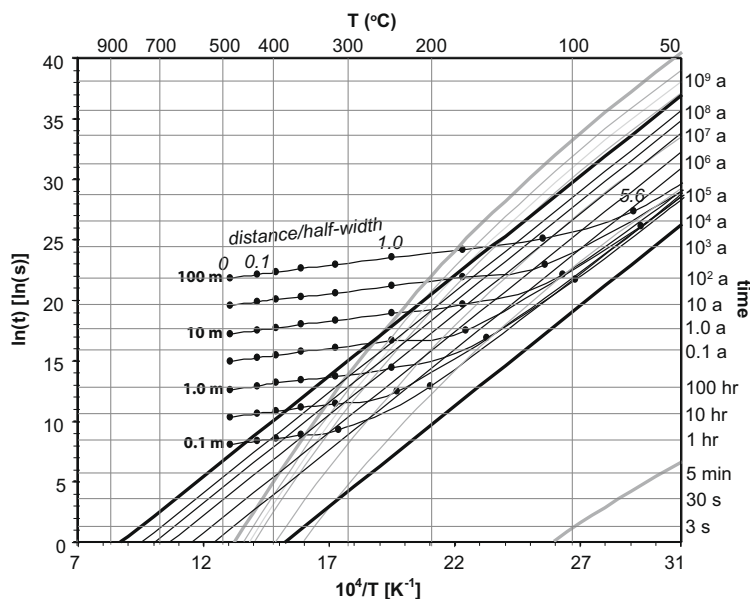


Fig. 10. Model trends of equivalent square pulse heating events for related samples at varying normalized distances from a central heat source of varying half-thickness (0.1–100 m) with initial  $T = 1000$  °C, initial wallrock  $T = 10$  °C, and (uniform) thermal diffusivity =  $0.61$  mm<sup>2</sup>/s; no latent heat (Delaney, 1987). Ambient conditions are 100 Myr at 10 °C. Symbols on model trends represent 0.25 log unit intervals in normalized distance from heat source. Grey and black solid lines at higher angles to labelled trends are AFT and apatite He fractional resetting contours, as in Fig. 5. Although this figure shows the square-pulse equivalent trends for spatially related samples resulting from dikes of varying thickness, the same approach could be used to constrain advective heat fluxes through veins or dikes whose preserved thickness is not simply related to heat flux.

the wildfire samples in Fig. 9 may arise from analytical errors or violations of the assumptions outlined above, they are also consistent with models requiring the accumulation of thermal effects from multiple wildfire and possibly spallation events affecting this  $\sim 200$ -cm<sup>2</sup> surface.

The example above illustrates the more general potential for modeling thermal perturbations caused by other types of heat sources. The magnitude and duration of heating of wallrocks by hydrothermal veins and magmatic dikes, for example, depends on the flux of material and heat through them, which is not necessarily observable from field relations. Ephemeral heating during brittle faulting is also highly variable and difficult to predict from field observations (e.g., Murakami et al., 2002; d'Alessio et al., 2003). Fig. 10 shows modeled square-pulse equivalent temperatures and durations for samples at varying distances from dikes of varying thickness (see caption for model details) intruded into wallrock with assumed ambient conditions of 10 °C for 100 Myr. As in the wildfire example, samples at increasing distances from the heat source yield increasing durations and decreasing temperatures of square-pulse equivalent perturbations. Each trend is consistent with a unique energy content of the heat source. In this example this is represented by instantaneous dike thickness, but this could also represent mass flux through a dike or vein.

#### 4.3. Implications of the apatite (U–Th)/He radiation-damage diffusion model for nonmonotonic thermal histories

A recent major advance in the interpretation of apatite (U–Th)/He ages is a He diffusion kinetic model that ac-

counts for decreasing diffusivity with increasing He concentration ([He]), as observed in both <sup>3</sup>He and <sup>4</sup>He diffusion experiments (Shuster et al., 2006). The model uses a multikinetic Arrhenius relation in which [He] is a proxy for the abundance of radiation-damage related “traps” with lower He diffusivity than undamaged parts of the crystal. Changes in  $E_a$  and  $D_0/a^2$  as a function of [He] are derived empirically from the experiments and incorporated into the mechanistic model. The multikinetic model results in a progressive increase in the apatite He  $T_c$  (for 10 °C / Myr) with increasing [He], from 53 °C at  $10^{-1}$  nmol <sup>4</sup>He/g, to 109 °C at  $10^3$  nmol <sup>4</sup>He/g. Most importantly for this study, this is accompanied by a systematic increase in  $E_a$ , from 121 to 148 kJ/mol (Shuster et al., 2006), compared with the  $E_a$  of 138 kJ/mol determined for Durango apatite (Farley, 2000) (Table 1).

The increasing  $E_a$  of He diffusion with higher [He] shifts fractional resetting contours in a pseudo-Arrhenius plot to higher temperatures (Fig. 11). This has an important effect on the relative resetting contours of the apatite He and AFT systems. In particular, the 99% resetting contour for the apatite He system for [He]  $> 10^2$  nmol/g is shifted to the higher temperature side of the complete resetting contour of the AFT system, for all temperatures and time-scales. Reheating events with square-pulse equivalent durations and temperatures in the grey field of Fig. 11 (between full AFT and apatite He resetting) completely reset the AFT system but only partially reset the apatite He system. Lower temperature reheating events may also partially reset the AFT system to significantly greater extents than the apatite He system, which would lead to apatite He ages

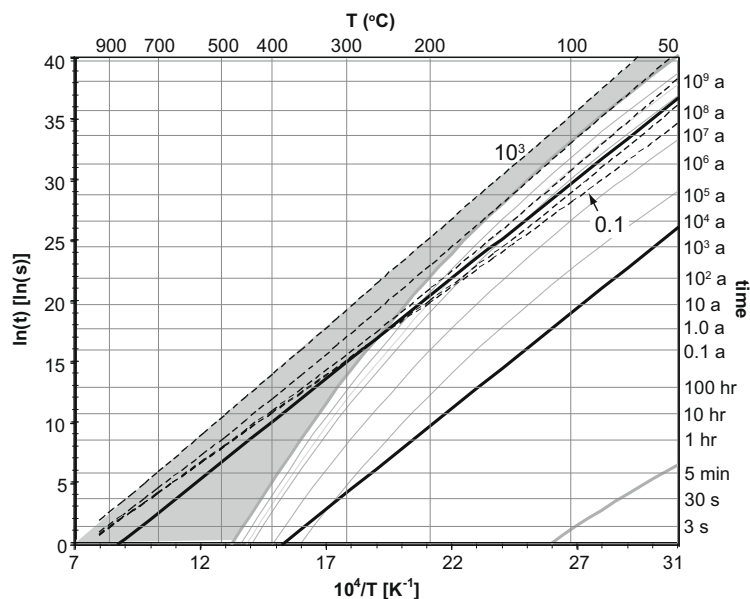


Fig. 11. Fractional resetting plot for He diffusion [solid lines: Durango apatite with  $a = 60 \mu\text{m}$ ; Farley (2000); dashed lines: radiation-damaged model of Shuster et al. (2006)] and fission-track annealing (grey lines) in apatite. AFT model uses curvilinear fanning model (RN composition) of Ketchum et al. (1999). The highest and lowest temperature dashed trends are radiation-damage models for apatites with  $10^{-1}$  and  $10^3 \text{ nmol } ^4\text{He/g}$ , respectively; intermediate dashed trends are shown for unit log increments. The grey field corresponds to square-pulse equivalent reheating episodes resulting in complete AFT resetting and only partial apatite He resetting. For the high-He apatite, this “inversion” is expected over a wide range of reheating histories, including those at low temperatures and long durations.

older than AFT ages (if the pre-heating AFT age was not much older than the He age). The difference between this situation and one assuming conventional He diffusion (i.e., that of Durango apatite) is that the reheating event need not require high- $T$ s and short durations, but may involve low- $T$  and long duration events, such as may result from a wide range of histories involving burial, top-down volcanic heating, or exposure to hydrothermal fluids. This may explain several examples of inverted apatite He–FT ages (Stockli et al., 2000; Emmel et al., 2007) which might otherwise require heating events too short and high- $T$  to be consistent with geologic evidence.

An important caveat in this analysis is that the kinetics of annealing of radiation damage that, in turn, controls the He diffusion are not yet known. If this damage is annealed at the same rate as, or more rapidly than, fission-track annealing, the phenomenon outlined above would be more complicated than depicted here. More work is needed to completely understand the kinetics of He diffusion and their relationships with  $[\text{He}]$  and radiation damage. Nevertheless, this analysis shows that nonmonotonic thermal histories may have nonintuitive effects on relative ages of thermochronometers with different kinetic properties, which cannot be simply understood by their relative  $T_c$ s.

#### 4.4. Meteorite thermal histories

Martian meteorite ALH84001 is an orthopyroxenite with Pb/Pb and Rb/Sr ages of  $\sim 4.0 \text{ Ga}$  (Borg et al., 1999), an  $^{40}\text{Ar}/^{39}\text{Ar}$  age of about  $3.9 \text{ Ga}$  (Turner et al., 1997; Bogard and Garrison, 1999), and a cosmogenic exposure age of  $\sim 15 \text{ Ma}$  (Nyquist et al., 2001). The latter is

interpreted as the timing of impact on and ejection from Mars (Swindle et al., 1995). The thermal history associated with impact is critical to hypotheses bearing on potential interplanetary transport of organic compounds and the origin of delicate paleomagnetic microdomain arrangements hypothesized to reflect an ancient Martian magnetic field, surface temperatures, and low-temperature escape and transport (Weiss et al., 2002; Shuster and Weiss, 2005).

Shuster and Weiss (2005) modeled Ar step-heating release data to interpret diffusion kinetics of the dominant K- and Ar-bearing phase, maskelynite. Its activation energy for Ar diffusion is low relative to most thermochronometers, and, combined with the inferred  $D_0/a^2$  and an assumed cooling rate of  $10 \text{ }^\circ\text{C}/\text{Myr}$ , yields a nominal  $T_c$  of less than  $10 \text{ }^\circ\text{C}$ . As shown by Shuster and Weiss (2005), the  $3.9\text{-Ga } ^{40}\text{Ar}/^{39}\text{Ar}$  age therefore requires a very low time-averaged temperature, consistent with low Martian surface temperatures and derivation from a shallow depths in the Martian crust. If the bulk of this Ar were lost in a single, recent impact event, such as that inferred to have ejected the meteorite from Mars at  $15 \text{ Ma}$ , the maskelynite Ar system would have experienced about 5–8% resetting. As shown in Fig. 12, this constrains the  $t$ – $T$  history associated with the hypothetical impact event to a family of square-pulse histories shown by the broad grey band. An additional constraint from another partially reset thermochronometer with a different activation energy is required to further constrain this event.

Min and Reiners (2007) measured ages of  $60 \text{ Ma}$  to  $1.8 \text{ Ga}$ , and a weighted mean age of  $830 \text{ Ma}$ , on phosphate (merrillite) grains from ALH84001, consistent with a range of diffusion domain sizes that were partially reset

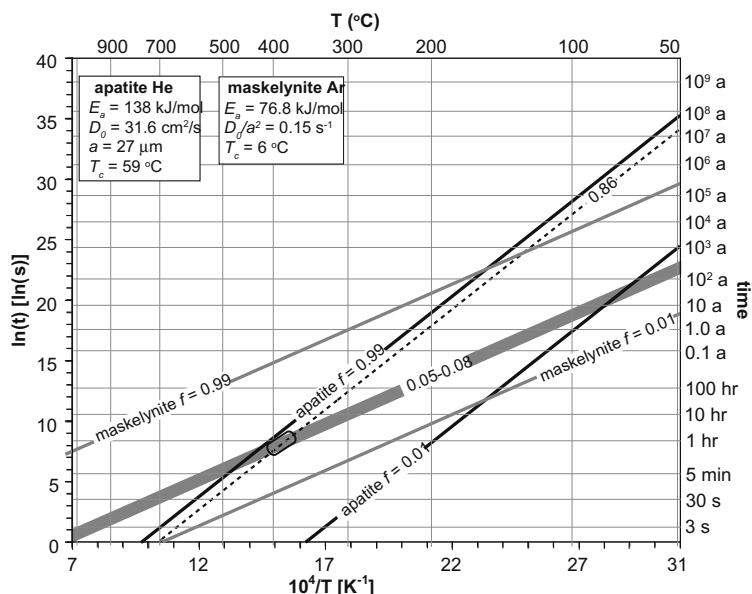


Fig. 12. Fractional resetting plot showing 1% and 99% fractional loss contours of the apatite He and maskelynite Ar systems [Table 1, but here with  $a = 27 \mu\text{m}$  for apatite He; see Min and Reiners (2007)], as a function of  $\ln(t)$  and inverse  $T$ . Dashed line is the 86% fractional loss contour for apatite He; thick grey band is 5–8% loss for maskelynite Ar. These represent the extents of resetting for the merrillite He and maskelynite Ar systems, based on analyses of bulk rock samples and single merrillite grains from Martian meteorite ALH84001 (Weiss et al., 2002; Shuster and Weiss, 2005; Min and Reiners, 2007), assuming negligible loss of He or Ar since 4.0 Ga and a single, recent reheating event. The square-pulse equivalent reheating event consistent with these data corresponds to  $\sim 400 \text{ }^\circ\text{C}$  for  $\sim 1 \text{ h}$ , a reasonable post-impact thermal history for a precursor meteorite to ALH84001 ejected from Mars at 15 Ma (Min and Reiners, 2007).

more recently than 60 Ma. Again assuming a single, recent impact and He loss event since 4.0 Ga, and assuming He diffusion kinetics of Durango apatite (Farley, 2000) [see Min and Reiners (2007) for detailed discussions on these points] this corresponds to about 86% He loss. Given the relative closure temperatures of the phosphate He and maskelynite Ar systems ( $\sim 65$  and  $\sim 6$   $^\circ\text{C}$ , respectively), the much older age of the  $^{40}\text{Ar}/^{39}\text{Ar}$  system therefore requires a significant reheating event in the thermal history of this meteorite. As shown by Min and Reiners (2007), the relative average fractional losses can be inverted to solve for the square-pulse equivalent thermal history representing a single recent event since 4.0 Ga. In this case, it corresponds to  $\sim 400 \text{ }^\circ\text{C}$  and a duration of tens of minutes to less than  $\sim 2 \text{ h}$  (intersection of fractional resetting contours in Fig. 11). This is consistent with a post-impact and post-ejection precursor body size larger than ALH84001 prior to delivery to Earth, in order to maintain relatively high temperatures on the order of 1 h. This analysis makes a number of assumptions, including that there was a single heating event after 4.0 Ga (the 15-Ma impact-ejection event) that caused all He and Ar loss from their carrier phases, that this event can be adequately approximated by a square-pulse equivalent event (subject to the uncertainties outlined in the previous section on non-square-pulse events), and that the kinetics of both systems are known accurately. These may not be true, but the general approach followed here could be adapted to situations involving more complex or multiple impact-heating scenarios (e.g., Min and Reiners, 2007).

#### 4.5. Metamorphic thermal histories

The kinetic crossovers in Fig. 4 show several potential examples of thermochronometer pairs that could potentially be used to deduce nonmonotonic cooling histories associated with metamorphism. Unlike plutonic rocks, which at least may have experienced only monotonic cooling, metamorphic rocks at the Earth's surface must have experienced at least one prograde–retrograde cycle. In some cases a metamorphic thermal history may have involved sufficient time at sufficiently high  $T$  to completely reset all thermochronometers, in which case they should record only the monotonic cooling path. But in some cases thermochronometers may be only partially reset, especially those with low  $E_a$ , and contain a pre-metamorphic age memory. Whether or not this occurs depends on, in addition to the kinetics of the system, how much time the rock spent near the highest temperatures, *not* the  $T_c$  of the system relative to the maximum metamorphic  $T$ .

The duration of metamorphic events, and in turn, whether thermochronometers are completely reset by them, is often ambiguous. Recent work on diffusion profiles in classic Barrovian metamorphic zones of Scotland show that the high temperatures associated with development of the characteristic metamorphic facies came in pulses shorter than  $10^6 \text{ yr}$  (and possibly significantly shorter), even in overall mountain building cycles lasting  $\sim 10^7 \text{ yr}$  (Agué and Baxter, 2007). These pulses were probably caused by short-lived magmatic or fluid-advection events. Similarly, recent work in the Western Gneiss Province of Norway leads to vastly discrepant estimates of the duration of

high- $T$  metamorphic events, from  $10^4$ – $10^5$  yr to more than  $10^7$  yr (Camacho et al., 2005, 2006; Bjornerud and Austrheim, 2006; Glodny et al., 2008), with the shorter timescale events again consistent with advection of heat by fluids moving through spatially restricted zones. Ague and Baxter (2007) summarized a variety of other studies deducing very short durations of peak metamorphic conditions, but point out that it is not known whether fast metamorphism is common and simply increasingly appreciated, or rare and identified in only a few circumstances. The potential for brief metamorphic events to incompletely reset some thermochronometers leads to the possibility of using the approaches outlined here to address this debate. Although several different systems, together with the use of diffusion profiles and other data, may be capable of addressing this, only the Rb/Sr system in micas is briefly discussed here, because micas are common minerals in metamorphic rocks, they appear to have relatively low  $E_a$  for this system, and they have led to vigorous debate surrounding these and broader issues about diffusion.

Rb/Sr ages of micas in metamorphic rocks are commonly observed to be “too old” to be consistent the inferred metamorphic history of their host rocks. Examples include high-grade metamorphic rocks in western Norway (e.g., Verschure et al., 1980; Kühn et al., 2000; Glodny et al., 2008), the central and eastern Alps (von Blanckenburg et al., 1989; Steck and Hunziker, 1994), and the Urals (Glodny et al., 2003). The preservation of pre-metamorphic or too-old Rb/Sr mica ages has been suggested to reflect (1) previously overestimated diffusivity of Sr in micas (e.g., von Blanckenburg et al., 1989); (2) complications of the Rb/Sr system arising from varying modes and kinetics of multiple equilibrating minerals (e.g., Ganguly and Ruiz, 1987; Jenkin et al., 1995, 2001; Jenkin, 1997); and (3) a general lack of thermally-activated diffusion in rocks without free fluids, and failure of thermochronologic theory (e.g., Villa, 1998; Kühn et al., 2000; Glodny et al., 2003, 2008).

The thermochronologic behavior of the Rb/Sr system in micas is complicated by exchange and diffusion among and within multiple phases (Ganguly and Ruiz, 1987; Jenkin et al., 1995, 2001; Jenkin, 1997). In addition, experimental constraints on diffusion kinetics are few and especially limited for white mica (Giletti, 1991; Jenkin et al., 1995; Jenkin, 1997; Hammouda and Cherniak, 2000). Nevertheless, available constraints, summarized Figs. 3 and 4 and Table 1, show that Sr diffusion in micas, which is probably the rate limiting parameter in Rb/Sr equilibration, has unusually low  $E_a$  relative to most other thermochronometers. Fig. 4 shows that in the range of  $10^3$ – $10^9$  yr and 300–900 °C, these systems have kinetic crossovers with many higher- $E_a$  systems including the Ar/Ar system in biotite, muscovite, and hornblende, and the U/Pb system in apatite and titanite. Rb/Sr in muscovite and Ar/Ar in hornblende, for example, which have nominal  $T_c$ s of ~520 and 570 °C, respectively, show a crossover at approximately 600 °C and  $10^7$  yr. Given that some studies have proposed peak metamorphic conditions with temperatures in this range, but timescales about two to three orders of magnitude lower (e.g., Camacho et al., 2005; Ague and Baxter, 2007), this raises the possibility that some “too-old” mica

Rb–Sr ages are simply partially reset, whereas other systems, including those with higher  $T_c$ s such as hornblende Ar/Ar, are fully reset and record only the retrograde path.

As noted above, although there are many potential complications to the thermochronologic behavior of the mica Rb/Sr systems, there are also many examples of too-old Rb/Sr micas in metamorphic rocks. One example comes from the western Tauern Window of the Eastern Alps, where von Blanckenburg et al. (1989) observed ages ranging from 20 to 7 Ma on a range of thermochronometric systems. Except for the phengite Rb/Sr ages, all of the other systems, as well as newer zircon and apatite FT data (Fugenschuh et al., 1997), were consistent with a single monotonic cooling history. In particular, the hornblende K/Ar system, which is thought to have a higher  $T_c$  than the phengite Rb/Sr system, had an age of 18 Ma, 2 Myr younger than the phengite Rb/Sr age. von Blanckenburg et al. interpreted this as requiring a significantly higher  $T_c$  for phengite Rb/Sr than previously thought (e.g., Purdy and Jäger, 1976). Increasing the phengite  $T_c$  by ~50 °C resulted in an acceptable monotonic cooling path beginning at about 20 Ma. However, another potential explanation is suggested by the kinetic crossover between the hornblende Ar and muscovite (as a proxy for white mica in general) Rb/Sr systems at approximately 600 °C and  $10^7$  yr (Fig. 4).

The thermal history of the western Tauern Window prior to ~20 Ma is poorly known, but Christensen et al. (1994) documented growth of garnet phenocrysts at temperatures of ~450–550 °C from 35–30 Ma, and as early as 60 Ma in some units. The fact that white mica Rb/Sr ages are consistently older than hornblende K/Ar ages in these rocks is consistent with a significant prograde heating event between prior to 20 Ma that resulted in complete resetting of the hornblende K/Ar system, but only partial resetting of the mica Rb/Sr system. Simple modeling using the kinetics and grain sizes in Table 1 shows that model histories involving temperatures greater than ~475 °C prior to 30 Ma and a ~5–10 Myr duration triangular heat pulse with a maximum temperature of ~650–675 °C at 20 Ma, reproduces well the ages in von Blanckenburg et al. (1989), including apparently “inverted” Rb/Sr mica and hornblende K/Ar ages. Fully exploring the plausibility of this scenario and its consistency with the large number of studies bearing on the  $P$ – $T$ – $t$  histories of various parts of the Tauern Window is beyond the scope of this paper. But this example provides an indication of how apparent kinetic age inversions and partial resetting extents could potentially be used for elucidating thermal histories of metamorphic events. Doing this with confidence, however, would require significantly better constraints on the kinetics of higher-temperature thermochronologic systems with contrasting activation energies (e.g., mica Rb/Sr).

## 5. SUMMARY AND CONCLUSIONS

Interpretation of thermochronologic data is typically made in the context of monotonic cooling, which permits use of the  $T_c$  concepts and often limits acceptable  $t$ – $T$  paths to a sufficiently small range to be geologically useful. Allowing for nonmonotonic thermal histories usually adds con-

siderable complexity and ambiguity to thermochronologic interpretations. But it also permits the potential identification of geologically important reheating events such as might occur during burial, metamorphism, exposure to hydrothermal fluids, brittle faulting, magmatism, and other processes. Contrasting kinetics of daughter product diffusion or annealing in different thermochronometers provides a potential way to diagnose and constrain durations and temperatures of reheating events. Systems with different activation energies display kinetic crossovers in diffusivity and fractional losses for reheating events. For some reheating events, systems with relatively high activation energies may experience greater fractional loss (resetting) extents than systems with lower activation energies, which can lead to younger ages for systems with higher  $T_c$ s, a observation that diagnoses a nonmonotonic cooling history. If both systems were partially reset by a reheating event, and fractional losses can be estimated from ages of the thermochronometers (which requires estimates of pre-event ages and post-event ingrowth), these can be combined with kinetic models of the systems to yield an estimate of the temperature and duration of the reheating event. Assuming a square-pulse form of the reheating event when actual pro- and retrograde paths are more gradual will generally underestimate the maximum temperature and duration of the event.

Analysis of single-grain apatite He and FT ages in samples subjected to recent wildfire heating in surficial bedrock shows that most samples require heating to  $\sim 300$ – $425$  °C for seconds to hours and an inverse correlation between temperature and duration of reheating, as expected for thermal cycles on rocks at varying distances from a heated free surface. Modeling of predicted square-pulse equivalent temperatures and durations for spatially related samples, however, shows that these samples likely record multiple heating events with variable magnitude, possibly combined with surface spallation from some parts of the exposed surface. Consideration of new radiation-damaged dependent He diffusion models for the apatite He system also suggest that nonmonotonic thermal histories, even those involving relatively low temperatures and long durations, may cause AFT ages older apatite He ages.

There are several thermochronometers showing kinetic crossovers for reheating events in ranges applicable to metamorphic thermal histories. The Rb/Sr system in micas may have particularly low activation energies, so that for certain temperatures it would require significantly longer durations to be completely reset than other systems with higher nominal  $T_c$ s, such as hornblende Ar/Ar. This may explain the common observation of “too-old” Rb/Sr mica ages in metamorphic rocks, and is consistent with emerging evidence for short durations of metamorphic heating in some classic localities.

The approach outlined here is based on contrasts in kinetic properties, particularly activation energy, of different thermochronometric systems. It follows that identification and resolution of nonmonotonic thermal histories of rocks would benefit from observations combining systems that respond to temperature changes in vastly different ways. Beyond thermochronometers, these include elemental diffusion profiles; magnetic properties, which have high

activation energies and are particularly sensitive to temperature (instead of duration) of heating events; thermal maturation indicators in organic compounds; and thermally stimulated luminescence.

#### ACKNOWLEDGMENTS

Acknowledgment is made to the Donors of the American Chemical Society Petroleum Research Fund for support of this research. This work was also supported by NSF grant EAR-0236965. This work benefitted from discussions with members of the Earth System Evolution Program of the Canadian Institute for Advanced Research (CIFAR). Rich Ketcham, Jay Ague, and Marty Grove provided constructive reviews that improved this manuscript and the development of ideas in it.

#### REFERENCES

- Ague J. J. and Baxter E. F. (2007) Brief thermal pulses during mountain building recorded by Sr diffusion in apatite and multicomponent diffusion in garnet. *Earth Planet. Sci. Lett.* **261**, 500–516.
- Baxter E. F. (2003) Quantification of the factors controlling the presence of excess  $^{40}\text{Ar}$  or  $^4\text{He}$ . *Earth Planet. Sci. Lett.* **216**, 619–634.
- Bjornerud M. G. and Austrheim H. (2006) Hot fluids or rock in eclogite facies metamorphism?. *Nature* **440** E4.
- Blackburn T. J., Stockli D. F. and Walker J. D. (2007) Magnetite (U–Th)/He dating and its application to the geochronology of intermediate to mafic volcanic rocks. *Earth Planet. Sci. Lett.* **259**, 360–371.
- Bogard D. D. and Garrison D. H. (1999) Argon-V-40 “ages” and trapped argon in Martian shergottites, Chassigny, and Allan Hills 84001. *Meteorit. Planet. Sci.* **34**, 451–473.
- Borg L. E., Connelly J. N., Nyquist L. E., Wiesmann Shih H. and Reese Y. (1999) The age of the carbonates in Martian meteorite ALH84001. *Science* **286**, 90–94.
- Camacho A., Lee J. K. W., Hensen B. J. and Braun J. (2005) Short-lived orogenic cycles and the eclogitization of cold crust by spasmodic hot fluids. *Nature* **435**, 1191–1196.
- Camacho A., Lee J. K. W., Hensen B. J., Braun J., Reply to Bjornerud M. G. and Austrheim H. (2006) Hot fluids or rock in eclogite facies metamorphism? *Nature* **440**, E4–E5.
- Cherniak D. J. (1993) Lead diffusion in titanite and preliminary results on the effects of radiation damage on Pb transport. *Chem. Geol.* **110**, 177–194.
- Cherniak D. J. (2000) Pb diffusion in rutile. *Contrib. Mineral. Petrol.* **139**, 198–207.
- Cherniak D. J., Lanford W. A. and Ryerson F. J. (1991) Lead diffusion in apatite and zircon using ion implantation and Rutherford backscattering techniques. *Geochim. Cosmochim. Acta* **55**, 1663–1673.
- Cherniak D. J., Watson E. B., Grove M. and Harrison T. M. (2004) Pb diffusion in monazite: a combined RBS/SIMS study. *Geochim. Cosmochim. Acta* **68**, 829–840.
- Cherniak D. J. and Watson E. B. (1992) A study of strontium diffusion in K-feldspar, Na–K feldspar and anorthite using Rutherford Backscattering Spectroscopy. *Earth Planet. Sci. Lett.* **113**, 411–425.
- Cherniak D. J. and Watson E. B. (2001) Pb diffusion in zircon. *Chem. Geol.* **172**, 1999–2017.
- Crank J. (1975) *The Mathematics of Diffusion*. Oxford University Press.
- Christensen J. N., Selverstone J., Rosenfeld J. L. and DePaolo D. J. (1994) Correlation by Rb–Sr geochronol-

- ogy of garnet growth histories from different structural levels within the Tauern Window, Eastern Alps. *Contrib. Mineral. Petrol.* **118**, 1–12.
- Dodson M. H. (1973) Closure temperature in cooling geochronological and petrological systems. *Contrib. Mineral. Petrol.* **40**, 259–274.
- d'Alessio M. A., Blythe A. E. and Burgmann R. (2003) No frictional heat along the San Gabriel fault, California: evidence from fission-track thermochronology. *Geology* **31**, 541–544.
- Delaney P. T. (1987) Heat transfer during emplacement and cooling of mafic dykes. In *Mafic Dyke Swarms* (eds. H. C. Halls and W. F. Fahrig). *Geol. Assoc. Can. Spec. Pap.* **34**, 31–46.
- Emmel B., Jacobs J., Crowhurst P. and Daszinnies M. C. (2007) Combined apatite fission-track and single grain apatite (U–Th)/He ages from basement rocks of central Dronning Maud Land (East Antarctica) – possible identification of thermally overprinted crustal segments? *Earth Planet. Sci. Lett.* **264**, 72–88.
- Farley K. A., Wolf R. A. and Silver L. T. (1996) The effects of long alpha-stopping distances on (U–Th)/He ages. *Geochim. Cosmochim. Acta* **60**, 4223–4229.
- Farley K. A. (2000) Helium diffusion from apatite: general behavior as illustrated by Durango fluorapatite. *J. Geophys. Res.* **105**, 2903–2914.
- Farley K. A. (2007) He diffusion systematics in minerals: evidence from synthetic monazite and zircon structure phosphates. *Geochim. Cosmochim. Acta* **71**, 4015–4024.
- Fechtig H. and Kalbitzer S. (1966) The diffusion of argon in potassium bearing solids. In *Potassium–Argon Dating* (eds. O. A. Schaeffer and J. Zahringer). Springer, pp. 68–106.
- Foland K. A. (1994) Argon diffusion in feldspars. In *Feldspars and Their Reactions* (ed. I. Parsons). Kluwer, Amsterdam, pp. 415–447.
- Fugenschuh B., Seward D. and Mancktelow N. (1997) Exhumation in a convergent orogen: the western Tauern Window. *Terra Nova* **9**, 213–217.
- Ganguly J. and Ruiz J. (1987) Time–temperature relation of mineral isochrons: a thermodynamic model, and illustrative examples for the Rb–Sr system. *Earth Planet. Sci. Lett.* **81**, 338–348.
- Ganguly J., Tirrone M. and Hervig R. L. (1998) Diffusion kinetics of Samarium and Neodymium in garnet, and a method for determining cooling rates of rocks. *Science* **281**, 805–807.
- Giletti B. J. (1974) Studies in diffusion I: argon in phlogopite mica. In *Geochemical Transport and Kinetics* (eds. A. W. Hofmann, B. J. Giletti, H. S. Yoder Jr. and R. A. Yund). Carnegie Inst Washington Yearb Publ 634, Washington DC, pp. 107–115.
- Giletti B. J. (1991) Rb and Sr diffusion in alkali feldspars, with implications for cooling histories of rocks. *Geochim. Cosmochim. Acta* **55**, 1331–1343.
- Glodny J., Austrheim H., Molina J. F., Rusin A. and Seward D. (2003) Rb/Sr record of fluid–rock interaction in eclogites: the Marun-Keu complex, Polar Urals, Russia. *Geochim. Cosmochim. Acta* **67**(22), 4353–4371.
- Glodny J., Kühn A. and Austrheim H. (2008) Diffusion versus recrystallization processes in Rb–Sr geochronology: isotopic relics in eclogite facies rocks, Western Gneiss Region, Norway. *Geochim. Cosmochim. Acta* **72**, 506–525.
- Grove M. and Harrison T. M. (1996)  $^{40}\text{Ar}^*$  diffusion in Fe-rich biotite. *Am. Mineral.* **81**, 940–951.
- Hammouda T. and Cherniak D. J. (2000) Diffusion of Sr in fluorophlogopite determined by Rutherford backscattering spectrometry. *Earth Planet. Sci. Lett.* **178**, 339–349.
- Harrison T. M. (1981) Diffusion of  $^{40}\text{Ar}$  in hornblende. *Contrib. Mineral. Petrol.* **78**, 324–331.
- Harrison T. M., Yin A., Grove M., Lovera O. M., Ryerson F. J. and Zhou X. (2000) The zedong window: a record of superposed tertiary convergence in Southeastern Tibet. *J. Geophys. Res.* **105**, 19211–19230.
- Jenkin G. R. T. (1997) Mode effects on cooling rate estimates from Rb–Sr data. *Geology* **25**, 907–910.
- Jenkin G. R. T., Rogers G., Fallick A. E. and Farrow C. M. (1995) Rb–Sr closure temperatures in bi-mineralic rocks; a mode effect and test for different diffusion models. *Chem. Geol. (Isot. Geosci.)* **122**, 227–240.
- Jenkin G. R. T., Ellam R. M., Rogers G. and Stuart F. M. (2001) An investigation of closure temperature of the biotite Rb–Sr system: the importance of cation exchange. *Geochim Cosmochim. Acta* **65**, 1141–1160.
- Ketcham R. A. (2005) Forward and inverse modeling of low-temperature thermochronometry data. *Rev. Mineral. Geochem.* **58**, 275–314.
- Ketcham R. A., Donelick R. A. and Carlson W. D. (1999) Variability of apatite fission-track annealing kinetics: III. Extrapolation to geological time scales. *Am. Mineral.* **84**, 1235–1255.
- Kühn A., Glodny J., Iden K. and Austrheim H. (2000) Retention of Precambrian Rb/Sr phlogopite ages through Caledonian eclogite facies metamorphism, Bergen Arc Complex, W-Norway. *Lithos* **51**, 305–330.
- Kurz M. D. and Jenkins W. J. (1981) The distribution of helium in oceanic basalt glasses. *Earth Planet. Sci. Lett.* **53**, 41–54.
- Laslett G. M., Green P. F., Duddy I. R. and Gleadow A. J. W. (1987) Thermal annealing of fission tracks in apatite, 2. A quantitative analysis. *Chem. Geol. (Isot. Geosci. Sect.)* **65**, 1–13.
- Lovera O. M., Grove M. and Harrison T. M. (2002) Systematic analysis of K-feldspar  $^{40}\text{Ar}/^{39}\text{Ar}$  step heating results II: relevance of laboratory argon diffusion properties to nature. *Geochim. Cosmochim. Acta* **66**, 1237–1255.
- McDougall I. and Harrison T. M. (1999) *Geochronology and Thermochronology by the  $^{40}\text{Ar}/^{39}\text{Ar}$  Method*, second ed. Oxford University Press, New York.
- Mitchell S. G. and Reiners P. W. (2003) Influence of wildfires on apatite and zircon (U–Th)/He ages. *Geology* **31**, 1025–1028.
- Min K. and Reiners P. W. (2007) High temperature Mars-to-Earth transfer of meteorite ALH84001. *Earth Planet. Sci. Lett.* **260**, 72–85.
- Morgan D. J. and Blake S. (2006) Magmatic residence times of zoned phenocrysts: introduction and application of the binary element diffusion modelling (BEDM) technique. *Contrib. Mineral. Petrol.* **151**, 58–70.
- Murakami M., Tagami T. and Hasebe N. (2002) Ancient thermal anomaly of an active fault system: zircon fission-track evidence from Nojima GSJ 750 m borehole samples. *Geophys. Res. Lett.* **29**, 2123. doi:10.1029/2002GL015679.
- Nicolescu S. and Reiners P. W. (2005) (U–Th)/He dating of epidote and andradite garnet. *Geochim. Cosmochim. Acta* **69**, 23.
- Nyquist L. E., Bogard D. D., Shih C.-Y., Greshake A., Stöffler D. and Eugster O. (2001) Ages and geologic histories of Martian meteorites. *Space Sci. Rev.* **96**, 105–164.
- Purdy J. W. and Jäger E. (1976) K Ar ages on rock forming minerals from the Central Alps. *Mem. Ist Geol. Min. Univ. Padova* **30**, 31.
- Quidelleur Z., Grove M., Lovera O. M., Harrison T. M., Yin A. and Ryerson F. J. (1997) The thermal evolution and slip history of the Renbu Zedong Thrust, southeastern Tibet. *J. Geophys. Res.* **102**, 2659–2679.

- Rahn M. K., Brandon M. T., Batt G. E. and Garver J. I. (2004) A zero-damage model for fission-track annealing in zircon. *Am. Mineral.* **89**, 473–484.
- Reiners P. W. and Brandon M. T. (2006) Using thermochronology to understand orogenic erosion. *Ann. Rev. Earth. Planet. Sci.* **34**, 419–466.
- Reiners P. W. and Farley K. A. (1999) He diffusion and (U–Th)/He thermochronometry of titanite. *Geochim. Cosmochim. Acta* **63**, 3845–3859.
- Reiners P. W., Spell T. L., Nicolescu S. and Zanetti K. A. (2004) Zircon (U–Th)/He thermochronometry: He diffusion and comparison with  $^{40}\text{Ar}/^{39}\text{Ar}$  dating. *Geochim. Cosmochim. Acta* **68**, 1857–1887.
- Reiners P. W., Thomson S. N., McPhillips D., Donelick R. A. and Roering J. J. (2007) Wildfire thermochronology and the fate and transport of apatite in hillslope and fluvial environments. *J. Geophys. Res.-Earth Surf.* **112**, F04001, doi: 10.1029/2007JF000759.
- Robbins G. A. (1972) Radiogenic argon diffusion in muscovite under hydrothermal conditions. M.S. Thesis, Brown University, Providence.
- Shuster D. L. and Farley K. A. (2005) Diffusion kinetics of proton-induced  $^{21}\text{Ne}$ ,  $^3\text{He}$ , and  $^4\text{He}$  in quartz. *Geochim. Cosmochim. Acta* **69**, 2349–2359.
- Shuster D. L., Farley K. A., Sistierson J. M. and Burnett D. S. (2003) Quantifying the diffusion kinetics and spatial distributions of radiogenic  $^4\text{He}$  in minerals containing proton-induced  $^3\text{He}$ . *Earth Planet. Sci. Lett.* **689**, 1–14.
- Shuster D. L., Vasconcelos P. M., Heim J. A. and Farley K. A. (2005) Weathering geochronology by (U–Th)/He dating of goethite. *Geochim. Cosmochim. Acta* **69**(3), 659–673.
- Shuster D. L., Flowers R. M. and Farley K. A. (2006) The influence of natural radiation damage on helium diffusion kinetics in apatite. *Earth Planet. Sci. Lett.* **249**, 148–161.
- Shuster D. L. and Weiss B. P. (2005) Martian surface paleotemperatures from thermochronology of meteorites. *Science* **309**, 594–597.
- Steck A. and Hunziker J. (1994) The tertiary structural and thermal evolution of the Central Alps-compressional and extensional structures in an orogenic belt. *Tectonophysics* **238**, 229–254.
- Stockli D. F., Farley K. A. and Dumitru T. A. (2000) Calibration of the apatite (U–Th)/He thermochronometer on an exhumed fault block, White Mountains, California. *Geology* **28**, 983–986.
- Swindle T. D., Grier J. A. and Burckland M. K. (1995) Noble gases in orthopyroxenite ALH84001: a different kind of martian meteorite with an atmospheric signature. *Geochim. Cosmochim. Acta* **59**, 793–801.
- Turner G., Knott S. F., Ash R. D. and Gilmour J. D. (1997) Ar–Ar chronology of the Martian meteorite ALH84001: evidence for the timing of the early bombardment of Mars. *Geochim. Cosmochim. Acta* **61**, 3835–3850.
- Villa I. M. (1998) Isotopic closure. *Terra Nova* **10**, 42–47.
- Verschure R. H., Andriessen P. A. M., Boelrijk N. A. I. M., Hebeda E. H., Maijer C., Priem H. N. A. and Verdurmen E. A. Th. (1980) On the thermal stability of Rb–Sr and K–Ar biotite systems: evidence from coexisting Sveconorwegian (ca 870 Ma) and Caledonian (ca 400 Ma) biotites in SW Norway. *Contrib. Mineral. Petrol.* **74**, 245–254.
- von Blanckenburg F., Villa I. M., Baur H., Morteani G. and Steiger R. H. (1989) Time calibration of a PT-path from the Western Tauern Window, Eastern Alps: the problem of closure temperatures. *Contrib. Mineral. Petrol.* **101**, 1–11.
- Wartho J.-A., Kelley S. P., Brooker R. A., Carroll M. R., Villa I. M. and Lee M. R. (1999) Direct measurement of Ar diffusion profiles in a gem-quality Madagascar K-feldspar using the ultra-violet laser ablation microprobe (UVLAMP). *Earth Planet. Sci. Lett.* **170**, 141–153.
- Weiss B. P., Shuster D. L. and Stewart S. T. (2002) Temperature on Mars from  $^{40}\text{Ar}/^{39}\text{Ar}$  thermochronology of ALH84001. *Earth Planet. Sci. Lett.* **201**, 465–472.

Associate editor: Bernard Marty